ChemComm

COMMUNICATION

View Article Online
View Journal | View Issue

Cite this: *Chem. Commun.*, 2025, **61**, 14693

Received 5th March 2025,
Accepted 18th August 2025

DOI: 10.1039/d5cc01220a

rsc.li/chemcomm

Electrocatalytic CO_2 reduction with an immobilized iron complex on gas diffusion electrodes

Maria B. Brands,[a] James L. Marden,[a] Kaijian Zhu,[b] Annemarie Huijser[b] and Joost N. H. Reek *[a]

The immobilization of molecular electrocatalysts on gas diffusion electrodes (GDEs) overcomes mass transport limitations inherent to solution-phase CO_2 reduction. We report the immobilization of the molecular FeTDHPP catalyst on a GDE *via* supramolecular π–π interactions, achieving a 50-fold catalytic activity increase compared to solution-phase performance.

The goal to mitigate CO_2 emissions has spurred interest in CO_2 conversion technologies, resulting in the discovery of promising first-row transition metal electrocatalysts.[1–4] In terms of Faraday efficiency (FE), heterogeneous catalysts are typically outperformed by molecular organometallic complexes, which consist of a metal centre coordinated to a tuneable ligand, resulting in a well-defined catalytic center. By optimization of molecular complexes, CO_2 reduction with FEs of >95% to a single product can be achieved.[5] On the other hand, the attained current densities with these complexes are limited and therefore rarely reported. Instead, the catalytic activity is commonly reported as the turnover frequency (TOF) per catalytic centre, which can vary between 6 h^{-1} and 10^6 s^{-1}.[6] This activity is often evaluated with the molecular catalysts dissolved in the solution phase using a three-electrode setup.[6] CO_2 reduction requires that the four crucial reaction components – the catalyst, CO_2, electrons and protons – are in proximity, which is at the electrode surface. Such a setup is suboptimal, as only a small fraction of the bulk catalyst in solution determines the overall average activity per catalytic site (*i.e.*, only the catalysts that reside in the reaction-diffusion layer).[6,7] Furthermore, this setup suffers from mass transport limitations of the poorly dissolving CO_2 (0.033 M in water under ambient conditions),[1] which may limit catalytic turnover rates. Finally, due to the limited substrate availability, undesired side reactions can occur, such as catalyst decomposition or hydrogen evolution. Arguably, the commonly used setup to evaluate the performance of molecular electrocatalysts is far from ideal, since the catalyst suffers strongly from mass-transfer and diffusion limitations.

In recent years, gas diffusion electrodes (GDEs) have been explored for CO_2 reduction, especially in the field of heterogeneous catalysis (Fig. 1).[8–12] These electrodes allow gaseous CO_2 to diffuse through the electrode, which overcomes CO_2 mass transport limitations resulting in high CO_2 availability at the electrode that would be impossible to reach *via* dissolution under ambient conditions. These benefits can also hold for molecular electrocatalysts, if they are immobilized on the GDE surface. The catalysts are then preorganized at the place where the substrates and electrons come together. In this different microenvironment, where mass transport limitations are less significant, the intrinsic performance of the catalyst for CO_2 reduction can be measured more precisely and is often higher than the performance observed in solution.[13]

In the pioneering work of Brookhart and co-workers, a pyrene-functionalized iridium pincer complex was immobilized on a GDE.[14] As a result, CO_2-to-formate conversion could be achieved with turnover frequencies up to 900 min^{-1}, at relatively high current densities (15.6 mA cm^{-2}), while maintaining good selectivity to formate as a product (83%). In 2019, Robert and co-workers incorporated various molecular catalysts, such as CoPc, in a Nafion matrix on GDEs and reached high CO_2-to-CO reduction efficiency.[15,16] Reaching a FE of >95% at a current density of 150 mA cm^{-2} with the CoPc catalyst, their work placed the performance of molecular electrocatalysts on GDEs on par with classic heterogeneous catalysts on GDEs. This setup performed orders of magnitude better than earlier reports on the performance of the state-of-the-art molecular FeTDHPP (iron 5,10,15,20-tetrakis(2′,6′-dihydroxyphenyl)-porphyrin) catalyst in solution.[7]

The immobilization of molecular catalysts in a Nafion framework (Fig. 2) is arguably a revolutionary step forwards.[17–25] Nevertheless, part of the catalyst molecules are still outside the reaction-diffusion

[a] *Homogeneous, Supramolecular and Bio-Inspired Catalysis Van 't Hoff Institute for Molecular Sciences, University of Amsterdam, Science Park 904, 1098 XH Amsterdam, the Netherlands. E-mail: j.n.h.reek@uva.nl*
[b] *MESA+ Institute for Nanotechnology, University of Twente, Hallenweg 23, 7522 NH, Enschede, the Netherlands*

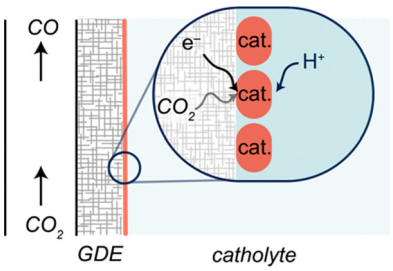

Fig. 1 The working principle of a GDE in electrochemical CO_2 reduction.

layer[26] and thus inaccessible for reduction by the electrode. Catalyst molecules can aggregate in the ionomer matrix,[27] impeding exposure of catalytic sites, which can hinder accessibility to CO_2.[28] We hypothesize that the catalyst can perform more efficiently (at lower loadings and higher activities per site) if the catalyst is directly immobilized on the GDE. In this work, we report the immobilization of the molecular FeTDHPP catalyst on a GDE *via* supramolecular π–π stacking (Fig. 3) and compared its catalytic performance in the CO_2 reduction reaction to earlier reports.

The FeTDHPP catalyst was synthesized according to a reported procedure and characterized with high resolution mass spectrometry, UV-vis spectroscopy and cyclic voltammetry.[7] The obtained characterization data agree with the literature, as detailed in the SI. Immobilization of the catalyst was achieved by deposition of multi-walled carbon nanotubes (MWCNTs) on a carbon paper-based GDE, leading to a material with large aromatic surfaces functioning as anchoring sites for the FeTDHPP catalyst *via* π–π stacking.[14,29–36] The structural changes after MWCNT deposition were characterized *via* scanning electron microscopy. The deposition of the catalyst resulted in a catalyst loading of 9.2×10^{-9} mol cm^{-2} (or 0.5 μg cm^{-2} Fe), as determined by UV-vis spectroscopy (SI). After confirming the catalytic activity of FeTDHPP in the aqueous environment (SI), the performance of this FeTDHPP-GDE in a custom-made flow reactor was explored,[37] *via* chronoamperometry

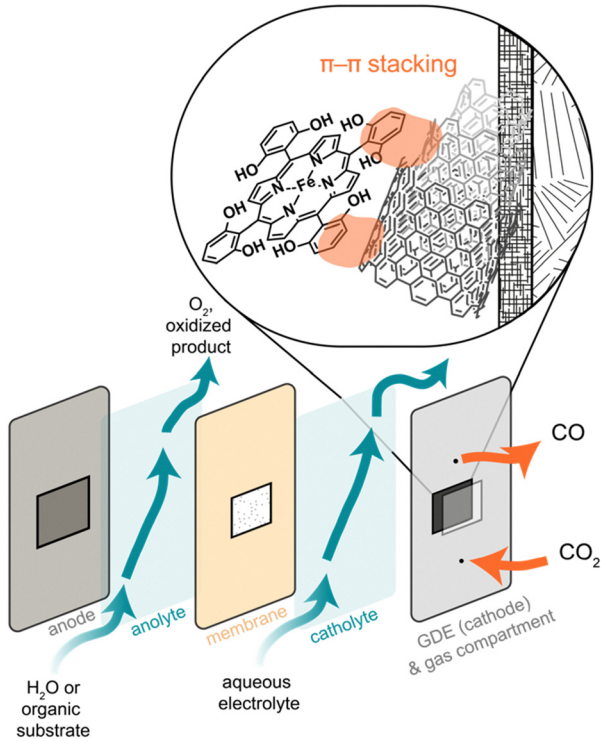

Fig. 3 Supramolecular immobilization of FeTDHPP on the GDE in an electrochemical CO_2 reduction flow cell.

and chronopotentiometry. In the three-compartment cell, the anolyte and catholyte compartments were separated by an anion exchange membrane, and the gas compartment and the catholyte were separated by the GDE. The electrolytes were circulated using a peristaltic pump. The CO_2 was supplied to the gas compartment *via* a single pass flow system, controlled by a mass flow controller (MFC) at a flow rate of 7.4 mL min^{-1}, and directed across the back side of the GDE. Effluent gases coming from the gas compartment were analysed by gas

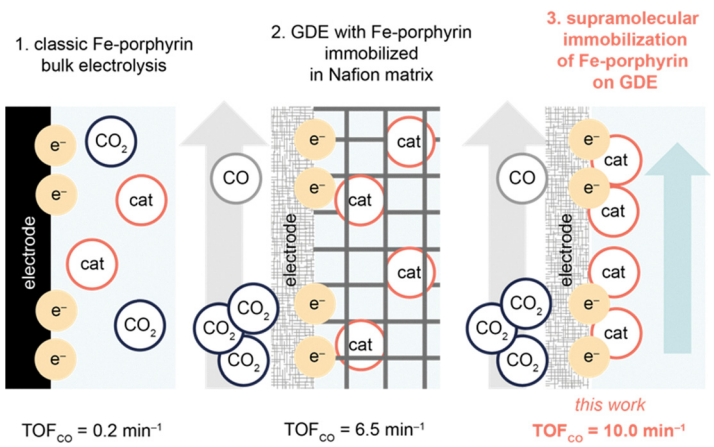

Fig. 2 Different ways that molecular catalysts have been studied in the electrochemical reduction of CO_2 to CO and their corresponding average TOF over the course of the experiment: (1) the approach reported by Robert and co-workers in 2012,[7] using FeTDHPP as the catalyst; (2) the approach reported by Robert and co-workers, using FeTNT (5,10,15,20-tetrakis(4-trimethylammonio-phenyl)-porphyrin tetrachloride) immobilized in a Nafion matrix on a GDE as the catalyst (0.5 M $NaHCO_3$);[15,16] and (3) the approach reported in this work, using FeTDHPP as the catalyst on a GDE *via* supramolecular immobilization (0.5 M $NaHCO_3$).

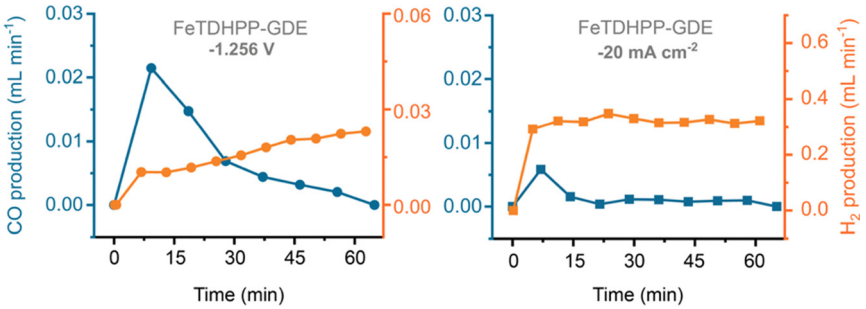

Fig. 4 Analyses of the produced gases over time during bulk electrolyses of the FeTDHPP-GDE. The CO production is given in blue on the left axes, and the H_2 production in orange on the right axes, both in mL min^{-1}. Left: CPE of the FeTDHPP-GDE at −1.256 V *vs.* Ag/AgCl; right: CCE of the FeTDHPP-GDE at −20 mA cm^{-2}.

chromatography. More details on the flow setup can be found in the SI.

Bulk electrolyses were carried out using the FeTDHPP-GDE at a constant potential (CPE) of −1.256 V *vs.* Ag/AgCl (Fig. 4, left) and at a constant current (CCE) of −20 mA cm^{-2} (Fig. 4, right). The CO production rate is given in blue and the H_2 evolution rate in orange. Additional experiments at 100 mA cm^{-2} and blank experiments with the GDE are reported in the SI.

The FeTDHPP-GDE displayed substantial activity in CO_2 reduction when a potential of −1.256 V was applied. CO was produced at an initial rate of 21.5 μL min^{-1}, corresponding to a $TOF_{max,CO}$ of 42 min^{-1} per FeTDHPP site. The CO production rate decreased over time, especially after 30 minutes, down to 2.0 μL min^{-1} (at 55 minutes), corresponding to a TOF of 4 min^{-1}. The catalyst reached an average TOF_{CO} of 10 min^{-1} (597 h^{-1}), which is the highest activity of CO_2-to-CO reduction reported to date for the FeTDHPP catalyst.

The FeTDHPP-GDE was also active in CO_2 reduction during constant current electrolysis at −20 mA cm^{-2}. The CO production started at 5.8 μL min^{-1} (7 min) but quickly lowered to 1.5 μL min^{-1} (14 min) and stabilized around 1.0 μL min^{-1} for the remaining time of the experiment. The resulting $TOF_{max,CO}$ under these conditions was 11 min^{-1}, and an average TOF_{CO} of 3 min^{-1} (179 h^{-1}) was measured. Although more current flowed through the electrode during CCE, the CO production was significantly lower compared to CPE. At higher current densities, the system thus strongly favour the formation of H_2.

The FEs towards H_2 and CO depend on (1) the current density and (2) the progress of the electrolysis experiment. The reaction was more selective towards CO during CPE (FE_{CO} of 34% over 1 h) compared to CCE (FE_{CO} = 0.5%). Hydrogen was thus a major product in both experiments, and most of the electrons ended up in H_2 rather than CO. In CCE, the fixed current may drive alternative reductions if the CO_2 reduction catalyst cannot keep up. Such side reactions could occur in bare areas of the electrode (*i.e.*, areas not containing nanotubes; see Fig. S6) that promote hydrogen formation (Fig. S11), resulting in a lower FE_{CO} and CO production rate.

The selectivity of the FeTDHPP-GDE changed over the course of the experiments: a decrease in the CO production rate was observed, while the H_2 evolution rate increased. In the CPE, the FE_{CO} started around 70% (at 9 minutes) decreasing gradually to ±10% (at 56 minutes). During CCE, the FE_{CO} was already close to zero after 14 minutes. The selectivity shift from CO to H_2 thus occurred earlier at higher current densities. This observation could indicate that, over the course of the experiments, the CO_2 reduction catalyst decomposes or leaches from the electrode, after which H_2 production increases.

Since the H_2 production rates are lower in the presence of a catalyst compared to the blank electrode, even at the end of the experiment, we hypothesize that the catalyst decomposes to a species that is inactive for both CO and H_2 production. This hypothesis is supported by post-catalytic elemental analysis of Fe in the FeTDHPP-GDE, the blank MWCNT-GDE, and their respective catholytes (Table S3), showing that part of the catalyst leached into solution, while part remained attached to the GDE surface. Hydrogen formation is most likely originating from the carbon electrode itself as (1) the Fe-catalyst is inactive for water reduction in DMF, as discussed earlier (Fig. S5), although this selectivity could change with the different solvent system (neat aqueous electrolyte) of the flow cell, and (2) the FeTDHPP-GDE shows a lower hydrogen production compared to the blank electrode during the beginning of the experiment (Fig. S11), indicating that FeTDHPP does not catalyze hydrogen evolution.

Importantly, the FeTDHPP-GDE performed at an average turnover frequency of 10 min^{-1} per catalytic site compared to a TOF of 0.2 min^{-1} when FeTDHPP resides in solution, as reported in earlier studies.[7] The catalytic activity of FeTHDPP thus increased by a factor of more than 50 when immobilized on a GDE *via* supramolecular immobilization.

In conclusion, we immobilized the FeTDHPP catalyst on a GDE *via* supramolecular π–π interactions, without the need for synthetic adjustments to the catalyst and using commercially obtained electrode materials. Compared to catalysis in solution, the CO_2-to-CO reduction increased more than 50-fold upon application on a GDE. Immobilization of molecular catalysts on a GDE can thus alleviate the mass-transfer and diffusion limitations that are usually present in solution, and enable molecular catalysts to operate closer to their full potential. Nevertheless, the overall stability, selectivity and activity of the FeTDHPP-GDE should be improved before its practical application can be considered. For instance, increasing the catalyst

loading, covering bare GDE regions, and strengthening the catalyst–GDE interactions could enhance the performance of the electrode.[29,38,39] Clearly further development is needed, for example the presented approach may be extended to other aromatic or π-conjugated molecular catalysts, broadening the scope for future molecular GDEs.

J. R. and M. B. conceived the project, designed the experiments, analyzed the data and wrote the manuscript. J. M. and M. B. carried out the synthesis and electrolysis experiments, and conducted data collection. K. Z. carried out scanning electron microscopy, which was supervised by A. H. All authors commented on the manuscript. Elemental analysis was carried out by Mikroanalytisches Laboratorium Kolbe.

This work is part of the Advanced Research Center for Chemical Building Blocks (ARC CBBC), which is co-founded and co-financed by the Dutch Research Council (NWO) and the Netherlands Ministry of Economic Affairs and Climate Policy. Prof. Dr. Tom Burdyny is acknowledged for helpful discussions on the cell design and for providing the blueprints of his earlier reported cell. We thank C. Ederveen Janssen for his contributions to developing the electrochemical cell. E. Zuidinga is acknowledged for mass spectrometry measurements.

Conflicts of interest

There are no conflicts to declare.

Data availability

The data supporting this article have been included as part of the SI. See DOI: **https://doi.org/10.1039/d5cc01220a**

Notes and references

1 G. Wang, J. Chen, Y. Ding, P. Cai, L. Yi, Y. Li, C. Tu, Y. Hou, Z. Wen and L. Dai, *Chem. Soc. Rev.*, 2021, **50**, 4993.
2 K. E. Dalle, J. Warnan, J. J. Leung, B. Reuillard, I. S. Karmel and E. Reisner, *Chem. Rev.*, 2019, **119**, 2752.
3 W. Ma, S. Xie, T. Liu, Q. Fan, J. Ye, F. Sun, Z. Jiang, Q. Zhang, J. Cheng and Y. Wang, *Nat. Catal.*, 2020, **3**, 478.
4 H. Yang, Q. Lin, C. Zhang, X. Yu, Z. Cheng, G. Li, Q. Hu, X. Ren, Q. Zhang, J. Liu and C. He, *Nat. Commun.*, 2020, **11**, 593.
5 R. Francke, B. Schille and M. Roemelt, *Chem. Rev.*, 2018, **118**, 4631.
6 E. Boutin, L. Merakeb, B. Ma, B. Boudy, M. Wang, J. Bonin, E. Anxolabéhère-Mallart and M. Robert, *Chem. Soc. Rev.*, 2020, **49**, 5772.
7 C. Costentin, S. Drouet, M. Robert and J.-M. Savéant, *Science*, 2012, **338**, 90.
8 M. F. Philips, G. J. M. Gruter, M. T. M. Koper and K. J. P. Schouten, *ACS Sustainable Chem. Eng.*, 2020, **8**, 15430.
9 D. Higgins, C. Hahn, C. Xiang, T. F. Jaramillo and A. Z. Weber, *ACS Energy Lett.*, 2019, **4**, 317.
10 Y. C. Tan, W. K. Quek, B. Kim, S. Sugiarto, J. Oh and D. Kai, *ACS Energy Lett.*, 2022, **7**, 2012.
11 G. Li, T. Yan, X. Chen, H. Liu, S. Zhang and X. Ma, *Energy Fuels*, 2022, **36**, 4234.
12 D. Wakerley, S. Lamaison, J. Wicks, A. Clemens, J. Feaster, D. Corral, S. A. Jaffer, A. Sarkar, M. Fontecave, E. B. Duoss, S. Baker, E. H. Sargent, T. F. Jaramillo and C. Hahn, *Nat. Energy*, 2022, **7**, 130.
13 T. Burdyny and W. A. Smith, *Energy Environ. Sci.*, 2019, **12**, 1442.
14 P. Kang, S. Zhang, T. J. Meyer and M. Brookhart, *Angew. Chem., Int. Ed.*, 2014, **53**, 8709.
15 W. Braun, D. Joulie, B. Boudy, K. Torbensen and M. Robert, WO 2021/013530A1, 2021.
16 S. Ren, D. Joulié, D. Salvatore, K. Torbensen, M. Wang, M. Robert and C. P. Berlinguette, *Science*, 2019, **365**, 367.
17 B. Siritanaratkul, M. Forster, F. Greenwell, P. K. Sharma, E. H. Yu and A. J. Cowan, *J. Am. Chem. Soc.*, 2022, **144**, 7551.
18 K. Torbensen, C. Han, B. Boudy, N. von Wolff, C. Bertail, W. Braun and M. Robert, *Chem. – Eur. J.*, 2020, **26**, 3034.
19 X. Zhang, Y. Wang, M. Gu, M. Wang, Z. Zhang, W. Pan, Z. Jiang, H. Zheng, M. Lucero, H. Wang, G. E. Sterbinsky, Q. Ma, Y. G. Wang, Z. Feng, J. Li, H. Dai and Y. Liang, *Nat. Energy*, 2020, **5**, 684.
20 Z. Jiang, Z. Zhang, H. Li, Y. Tang, Y. Yuan, J. Zao, H. Zheng and Y. Liang, *Adv. Energy Mater.*, 2023, **13**, 2203603.
21 C. Eagle, G. Neri, V. L. Piercy, K. Younis, B. Siritanaratkul and A. J. Cowan, *Sustainable Energy Fuels*, 2023, **7**, 2301.
22 Y. Zhao, S. Wang, L. J. Zhu, M. J. Sun, T. Zhang and R. Cao, *ChemElectroChem*, 2022, **9**, e202200023.
23 M. Fang, L. Xu, H. Zhang, Y. Zhu and W. Y. Wong, *J. Am. Chem. Soc.*, 2022, **144**, 15143.
24 H. Bemana, M. McKee and N. Kornienko, *Chem. Sci.*, 2023, **14**, 13696.
25 L. Yao, K. E. Rivera-Cruz, N. Singh and C. C. L. McCrory, *Curr. Opin. Electrochem.*, 2023, **41**, 101362.
26 M. Abdinejad, A. Farzi, R. Möller-Gulland, F. Mulder, C. Liu, J. Shao, J. Biemolt, M. Robert, A. Seifitokaldani and T. Burdyny, *Nat. Catal.*, 2024, **7**, 1109.
27 S. Ren, E. W. Lees, C. Hunt, A. Jewlal, Y. Kim, Z. Zhang, B. A. W. Mowbray, A. G. Fink, L. Melo, E. R. Grant and C. P. Berlinguette, *J. Am. Chem. Soc.*, 2023, **145**, 4414.
28 X. Lv, Q. Liu, H. Yang, J. Wang, X. Wu, X. Li, Z. Qi, J. Yan, A. Wu, T. Cheng and H. Bin Wu, *Adv. Funct. Mater.*, 2023, **33**, 2301334.
29 A. Maurin and M. Robert, *J. Am. Chem. Soc.*, 2016, **138**, 2492.
30 M. Zannotti, R. Giovannetti, C. A. D'Amato and E. Rommozzi, *Spectrochim. Acta, Part A*, 2016, **153**, 22.
31 Y.-L. Zhao and J. F. Stoddart, *Acc. Chem. Res.*, 2009, **42**, 1161.
32 J. H. Zagal, S. Griveau, K. I. Ozoemena, T. Nyokong and F. Bedioui, *J. Nanosci. Nanotechnol.*, 2009, **9**, 2201.
33 T. Hasobe, S. Fukuzumi and P. V. Kamat, *J. Am. Chem. Soc.*, 2005, **127**, 11884.
34 H. Murakami, G. Nakamura, T. Nomura, T. Miyamoto and N. Nakashima, *J. Porphyrins Phthalocyanines*, 2007, **11**, 418.
35 X. X. Zhang, Z. Wu, X. X. Zhang, L. Li, Y. Li, H. Xu, X. Li, X. Yu, Z. Zhang, Y. Liang and H. Wang, *Nat. Commun.*, 2017, **8**, 14675.
36 P. D. Tran, A. Le Goff, J. Heidkamp, B. Jousselme, N. Guillet, S. Palacin, H. Dau, M. Fontecave and V. Artero, *Angew. Chem.*, 2011, **123**, 1407.
37 K. Liu, W. A. Smith and T. Burdyny, *ACS Energy Lett.*, 2019, **4**, 639.
38 F. Greenwell, G. Neri, V. Piercy and A. J. Cowan, *Electrochim. Acta*, 2021, **392**, 139015.
39 X. Lu, Y. Wu, X. Yuan, L. Huang, Z. Wu, J. Xuan, Y. Wang and H. Wang, *ACS Energy Lett.*, 2018, **3**, 2527.

